Hindawi
Mathematical Problems in Engineering
Volume 2020, Article ID 8656147, 15 pages
https://doi.org/10.1155/2020/8656147

Research Article

Three-Dimensional MHD Mixed Convection Flow of Casson Nanofluid with Hall and Ion Slip Effects

Wubshet Ibrahim[1] **and Temesgen Anbessa**[2]

[1]*Departement of Mathematics, Ambo University, Ambo, Ethiopia*
[2]*Departement of Mathematics, Wollega University, Nekemte, Ethiopia*

Correspondence should be addressed to Wubshet Ibrahim; wubshetib@yahoo.com

Received 26 February 2020; Revised 21 April 2020; Accepted 22 April 2020; Published 25 May 2020

Academic Editor: Sergey A. Suslov

The intention of the present study is to scrutinize the three-dimensional MHD mixed convection flow of Casson nanofluid over an exponentially stretching sheet using the impacts of Hall and ion slip currents. Moreover, the impacts of thermal radiation and heat source are considered in this study. The governing partial differential equations are transformed into a system of joined nonlinear ordinary differential equations using similarity transformations, and they are solved numerically employing a spectral relaxation method (SRM). The obtained results are contrasted with existing specific cases, and a reasonable harmony is established. The impacts of noteworthy physical parameters on the velocities, thermal and concentration distributions, skin friction coefficients, local Nusselt number, and local Sherwood number are investigated graphically. It is found that the rise in Casson fluid and magnetic field parameters reduce the velocity profiles along both $x-$ and $y-$ directions while the reverse tendency is observed with an increment in Hall, ion slip, and mixed convection parameters. Moreover, the increase in both radiation and heat source parameters enhances the temperature profile. It is also observed that both the skin friction coefficients reduced with an increase in Casson fluid, Hall, and ion slip parameters. Furthermore, the local Nusselt number enhances with an augment in radiation parameter, whereas the opposite trends of local Nusselt and Sherwood numbers are found with an increase in heat source parameter.

1. Introduction

Nanofluid is a kind of heat transport medium containing nanoparticles less than 100 nm which are consistently and steadily dispersed in a base fluid like water, oil, and ethylene glycol. These dispersed nanoparticles, mostly a metal or metal oxide, enormously improve the thermal conductivity of the nanofluid and enhance conduction and convection coefficients taking into consideration more heat transport. Reddy et al. [1] utilized finite element method to portray the impact of magnetohydrodynamic boundary layer stream and heat transport of nanofluid over a porous contracting sheet with divider mass suction and heat source/sink. They found that an increase in magnetic field and suction parameters leads to a rise in velocity profile, whereas opposite trends of the temperature and nanoparticle volume fraction profiles are observed. Also, Ramya et al. [2] numerically dissected the boundary layer viscous flow of nanofluids and heat transport over a nonlinearly extending sheet within the sight of a magnetic field utilizing Keller box method and found that the temperature profile and nanoparticle concentration increment with expanding values of the magnetic parameter. Zhao et al. [3] have explored the three-dimensional stream and heat transport of a nanofluid in the boundary layer region over a flat sheet extended constantly in two lateral directions utilizing homotopy analysis method (HAM), and they reported that the heat transport conductivity of the nanofluid is greater than that of the pure fluids. Furthermore, Khan et al. [4] examined the three-dimensional flow of nanofluid over a skin friction exponentially extending sheet

utilizing Keller box method. They reported the existence of remarkable Sparrow–Gregg-type hills for temperature profile in line with some range of parametric values. Moreover, Hayat et al. [5] computed three-dimensional boundary layer stream of viscous nanofluid over a bi-directional linearly extending sheet within the sight of Cattaneo–Christov two fold diffusion and reported that temperature and concentration profiles reduced with an increment in thermal and concentration relaxation parameters.

Recently, Shah et al. [6] investigated natural convection flow of hybrid nanofuid (Fe_3O_4 + MWCNT) with H_2O as base fluid in a porous media via control volume finite element method (CVFEM). They confirmed that the Nusselt number is an increasing function of porosity parameter, whereas opposite trend is noticed for Lorentz forces. Most recently, Shah et al. [7] scrutinized the effect of thermal radiation on Darcy–Forchheimer flow of micropolar ferrofluid with H_2O as base fluid and iron oxide (Fe_3O_4) as electromagnetite nanoparticles in a porous and dynamic sheet exposed to both suction and injection. They found that the velocity profile enhances with the increment in microrotation and electric field strength parameters for the stretching sheet, whereas the opposite result is observed for the shrinking sheet in both suction and injection cases. Moreover, Shah et al. [8] described the flow and heat diffusion of blood that carries the micropolar nanofluid of gold in a porous channel in presence of thermal radiation and found that the temperature distribution for the micropolar nanoparticles augments when the suction/injection parameter β is positive, i.e., $\beta > 0$ and it reduces when $\beta < 0$ for either moving or stationary walls of porous channel. Further, Alreshidi et al. [9] have discussed the time-independent and incompressible flow of MHD nanofluid past a permeable rotating disc with slip conditions. Besides, they studied the mass and heat diffusion with viscous dissipation effect and found that the fluid velocities diminish with the intensification in velocity slip, porosity, and magnetic parameters.

A mixed convection flow is the method of heat transport happened due to the consolidated impacts of free and forced convection flows. As of late, investigation of mixed convection boundary layer flow past a plate has increased striking consideration as it expects a vital part in numerous industrial and technological applications in nature, for example, streams in the sea and in the ambiance, sun oriented recipients exposed to wind currents, atomic reactors cooled during emergency shutdown, electronic devices cooled by fans, heat exchangers put in a low-velocity condition, etc. Izadi et al. [10] numerically contemplated the mixed convection heat transport and entropy generation of a nanofluid containing carbon nanotube flowing in a three-dimensional rectangular channel exposed to contradicted buoyant forces utilizing finite volume technique and found that with an expansion in the contradicted buoyancy parameter the nanofluid velocity close to the channel divider definitely lessens and, in this way, causes a decrease in the Nusselt number. Also, numerical simulation of mixed convection heat transport in a lid driven triangular hole filled with power law nanofluid and with an opening was performed under the impact of a slanted magnetic field by Selimefendigil and Chamkha [11]. They found that average heat transport reduces with Hartmann number, and in the company of magnetic field heat transfer rate is superior for dilatant fluid, while without the magnetic field a pseudoplastic fluid provides the maximum value of average heat transport. Most recently, numerous scholars concentrated on the examination of mixed convection flow of fluids by taking different angles and geometries [12–14].

Non-Newtonian fluids has obtained significant attention because of its wide range of applications in different industries, for example, structure of strong lattice heat, atomic waste transfer, synthetic synergist reactors, geothermal energy creation, ground water hydrology, transpiration cooling, oil supplies, and so forth. These fluids are progressively confounded when contrasted with Newtonian fluids because of nonlinear connection among stress and strain rate. Numerous models have been proposed for the investigation of non-Newtonian liquids, however, yet not a solitary model is built up that displays all properties of non-Newtonian fluids. Among various non-Newtonian fluids, Casson fluid is the most famous fluid which has many applications in nourishment handling, metallurgy, drilling activities, and bio-engineering tasks. Casson fluid is a shear thinning fluid which is accepted to have a limitless viscosity at zero rate of shear, a yield stress underneath which no flow happens and a zero viscosity at a boundless rate of shear. Some common examples of Casson fluid are honey, tomato sauce, jelly, soup, concentrated fruit juices, blood, and so on. Casson fluid model is a non-Newtonian fluid with yield stress which is extensively used for modeling blood flow in narrow arteries. Furthermore, Casson fluid possesses yield stress and has great importance in polymer processing industries and biomechanics. Hayat et al. [15] considered the mixed convection stream of Casson nanofluid over an extending surface in nearness of thermal radiation, heat source/sink, and first order chemical reaction. They reported that thermal boundary layer thickness is an increasing function of thermal radiation and internal heat generation. Moreover, Concentration distribution and associated boundary layer thickness increase with the increment in generative chemical reaction while reverse tendency is observed for destructive chemical reaction. Also, Kamran et al. [16] numerically examined Casson nanofluid past flat extending surface with magnetic impact and Joule heating considering slip and thermal convective boundary conditions utilizing Keller box method and they established that the effect of expanding Hartmann number resulted in the decline of both Sherwood and Nusselt number. Afify [17] numerically researched the effects of multiple slips with viscous dissipation on the boundary layer stream and heat transfer of a Casson nanofluid over an extending surface utilizing a shooting strategy with fourth-order Runge–Kutta integration scheme and they found inverse impact with generative chemical reaction and concentration slip

parameter. Recently, boundary layer flow of Casson nanofluids stream over various geometries was considered by numerous authors in references [18–24].

The investigation of MHD flows, the Hall current and ion slip relations in Ohms law have been disregarded in order to effortlessly lead scientific examination of the flow. Nevertheless, the result of the Hall current and ion slip is significant within the sight of a high magnetic field. Thus, in various characteristic conditions, it is fundamental to involve the impact of Hall current and ion slip terms of the magnetohydrodynamics articulations. Attributable to these realities, numerous investigations have been accounted for MHD streams within the sight of Hall and ion slip currents. Accordingly, Nawaz et al. [25] have investigated the Hall and ion slip impacts on three-dimensional combined free and forced convection flow of a Maxwell liquid over an extending vertical surface and they reported that the Hall parameter has similar impacts on both tangential and lateral velocities whereas the ion slip parameter has opposite impacts on both velocities. In addition, Nawaz and Zubair [26] studied the Hall and ion slip effects on three-dimensional flow equations of nano-plasma fluid in the company of homogeneous applied magnetic field and found that the inclusion of copper (Cu) and silver (Ag) nanoparticles greatly influences the velocity components and temperature of the nano-plasma. Some more investigations related to Hall and ion slip currents can be found in references [27–29].

Thermal radiation assumes a significant role in manufacturing industries for the design of atomic power plants and a few designing applications. Because of its essential applications various scientists have given their consideration to thermal radiation impact. Hayat et al. [30] scrutinized the impact of thermal radiation on three-dimensional mixed convection stream of viscoelastic fluid and reported that mixed convection parameter has opposite effect on velocity and temperature boundary layers. Makanda et al. [31] investigated the impacts of radiation on MHD natural convection flow of Casson fluid from a horizontal circular cylinder with partial slip in non-Darcy permeable medium and they established that both velocity and temperature profiles are increasing functions of the radiation parameter. Ullah et al. [32] numerically examined the results of chemical reaction on hydromagnetic free convection flow of Casson nanofluid induced as a result of nonlinearly extending sheet immersed in a permeable medium under the impact of convective boundary condition and thermal radiation. They found that Casson fluids are superior to manage the temperature and nanoparticle concentration as contrasted to Newtonian fluid for nonlinearly extending sheet. The inclusive references and in detail understanding on thermal radiation can be read in recent articles [33–37].

The aim of the present study is to investigate the Hall and ion slip impacts on the flow of MHD mixed convection flow of Casson nanofluid in presence of thermal radiation and heat source. Up to the authors' knowledge, there is no work is reported like the investigation of three-dimensional mixed convection flow of Casson nanofluid over an exponentially stretching sheet under the effect of Hall and ion slip currents. Along these lines, inspiration of the present examination is to direct the Hall and ion slip effects for mixed convection flow of Casson nanofluid over an exponentially stretching sheet employing spectral relaxation method. In particular, the study of the effects of mixed convection, Hall, ion slip, thermal radiation, and heat source parameters makes this work a novel one.

2. Mathematical Formulation

Consider the steady three-dimensional incompressible mixed convection flow of Casson nanofluid over an exponentially extending sheet in two lateral directions. The sheet is situated at $z = 0$ and the flow is restricted to $z \geq 0$. The fluid is electrically conducted by a consistent applied magnetic field B_0 in the $z-$direction orthogonal to the $xy-$plane. The induced magnetic field is ignored under the supposition of small magnetic Reynolds number. Suppose the velocities of the sheet along $x-$and $y-$directions be $U_w(x, y) = U_0 e^{(((x+y)/L))}$ and $V_w(x, y) = V_0 e^{(((x+y)/L))}$, respectively, where U_0 and V_0 are constants. The sheet is kept up at temperature $T_w(x, y) = T_\infty + T_0 e^{(n(x+y)/2L)}$ and the concentration $C_w(x, y) = C_\infty + C_0 e^{(n(x+y)/2L)}$ where T_0 and C_0 are constants, and T_∞ and C_∞ are the ambient values of temperature and concentration, respectively, as shown in Figure 1.

The rheological equation of state for an isotropic and incompressible flow of Casson nanofluid can be composed as [23, 36, 38]

$$\tau_{ij} = \begin{cases} 2\left(\mu_B + \dfrac{P_y}{\sqrt{2\pi}}\right)e_{ij}, & \pi > \pi_c, \\ 2\left(\mu_B + \dfrac{P_y}{\sqrt{2\pi_c}}\right)e_{ij}, & \pi < \pi_c, \end{cases} \tag{1}$$

where $\pi = e_{ij}e_{ij}$ and e_{ij} is the $(i, j)^{\text{th}}$ component of the deformation rate, π is the product of the component of deformation rate with itself, π_c is a critical value of this product based on the non-Newtonian model, μ_B is the plastic dynamic viscosity of the Casson fluid, and P_y is the yield stress of the fluid.

The generalized Ohm's law with Hall and ion slip consequences is given by [39–41]

$$\mathbf{J} = \sigma(\mathrm{E} + (\mathbf{V} \times \mathbf{B})) - \frac{\omega_e \tau_e}{B_0}(\mathbf{J} \times \mathbf{B}) + \frac{\omega_e \tau_e \beta_i}{B_0^2}(\mathbf{J} \times \mathbf{B}) \times \mathbf{B}, \tag{2}$$

where $\mathbf{J} = (J_x, J_y, J_z)$ is the current density vector, $\mathbf{E}$ is the intensity vector of the electric field, $\mathbf{V}$ is the velocity vector, $\mathbf{B}$

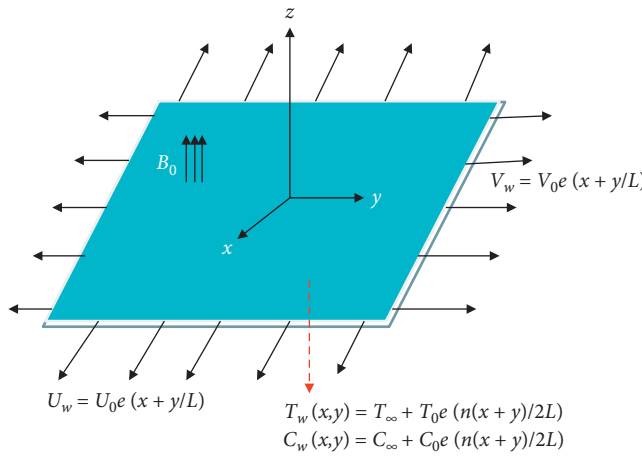

Figure 1: Physical model of the flow problem.

is the magnetic field, ω_e is the cyclotron frequency, and τ_e is the electrical collision time.

Thus, with the above assumptions and under the standard boundary layer suppositions, the equations governing the conservations of mass, momentum, energy, and nanoparticles mass are [26, 40–43]

$$\frac{\partial u}{\partial x} + \frac{\partial v}{\partial y} + \frac{\partial w}{\partial z} = 0, \tag{3}$$

$$u\frac{\partial u}{\partial x} + v\frac{\partial u}{\partial y} + w\frac{\partial u}{\partial z} = v\left(1 + \frac{1}{\beta}\right)\frac{\partial^2 u}{\partial z^2} + g\left[\beta_t (T - T_\infty) + \beta_c (C - C_\infty)\right] + \frac{\sigma B_0^2}{\rho\left(\alpha_e^2 + \beta_e^2\right)} \cdot (\beta_e v - \alpha_e u), \tag{4}$$

$$u\frac{\partial v}{\partial x} + v\frac{\partial v}{\partial y} + w\frac{\partial v}{\partial z} = v\left(1 + \frac{1}{\beta}\right)\frac{\partial^2 v}{\partial z^2} - \frac{\sigma B_0^2}{\rho\left(\alpha_e^2 + \beta_e^2\right)}(\beta_e u + \alpha_e v), \tag{5}$$

$$u\frac{\partial T}{\partial x} + v\frac{\partial T}{\partial y} + w\frac{\partial T}{\partial z} = \alpha\frac{\partial^2 T}{\partial z^2} - \frac{1}{(\rho C)_f}\frac{\partial q_r}{\partial z} + \frac{Q_0}{(\rho C)_f}(T - T_\infty) + \tau\left[D_B\left(\frac{\partial C}{\partial z}\right)\left(\frac{\partial T}{\partial z}\right) + \left(\frac{D_T}{T_\infty}\right)\left(\frac{\partial T}{\partial z}\right)^2\right], \tag{6}$$

$$u\frac{\partial C}{\partial x} + v\frac{\partial C}{\partial y} + w\frac{\partial C}{\partial z} = D_B\left(\frac{\partial^2 C}{\partial z^2}\right) + \left(\frac{D_T}{T_\infty}\right)\left(\frac{\partial^2 T}{\partial z^2}\right), \tag{7}$$

where $u, v,$ and w are the velocity components along the $x-$, $y-$, and $z-$ directions, respectively.

The boundary conditions for the considered flow problem are

$$\begin{aligned} u &= U_w, \\ v &= V_w, \\ w &= 0, \\ T &= T_w, \\ C &= C_w, \\ &\text{at } z = 0, \\ u &\longrightarrow 0, \\ v &\longrightarrow 0, \\ T &\longrightarrow T_\infty, \\ C &\longrightarrow C_\infty, \\ &\text{as } z \longrightarrow \infty, \end{aligned} \tag{8}$$

where $U_w = U_0 e^{(x+y/L)}, V_w = V_0 e^{(x+y/\ L)}, T_w(x, y) = T_\infty + T_0 e^{(n(x+y)/2L)}$, and $C_w(x, y) = C_\infty + C_0 e^{(n(x+y)/2L)}$.

The radiative heat flux q_r expressed in relation to Rosseland approximation is set as

$$q_r = \frac{-4\sigma^*}{3k^*}\frac{\partial T^4}{\partial z}, \tag{9}$$

where σ^* is the Stefan-Boltzmann constant and k^* is the mean absorption coefficient. T^4 can be conveyed as linear function of temperature. By expanding T^4 in a Taylor series about T_∞ and disregarding higher terms, we can write

$$T^4 \cong 4T_\infty^3 - 3T_\infty^4. \tag{10}$$

Substituting equations (9) and (10) into equation (6), we obtain

$$u\frac{\partial T}{\partial x}+v\frac{\partial T}{\partial y}+w\frac{\partial T}{\partial z}=\alpha\frac{\partial^2 T}{\partial z^2}+\frac{16\sigma^* T_\infty^3}{3k^*(\rho C)_f}\frac{\partial^2 T}{\partial z^2}+\frac{Q_0}{(\rho C)_f}\cdot(T-T_\infty)+\tau\left[D_B\left(\frac{\partial C}{\partial z}\right)\left(\frac{\partial T}{\partial z}\right)+\left(\frac{D_T}{T_\infty}\right)\left(\frac{\partial T}{\partial z}\right)^2\right]. \tag{11}$$

Use the following dimensionless variables [44, 45]:

$$\begin{aligned}
u&=U_0e^{(x+y/L)}f',\\
v&=U_0e^{(x+y/L)}g',\\
w&=-\sqrt{\frac{\nu U_0}{2L}}e^{(x+y/2L)}(f+\eta f'+g+\eta g'),\\
T&=T_\infty+T_0e^{(n(x+y)/2L)},\\
C&=C_\infty+C_0e^{(n(x+y)/2L)},\\
\eta&=\sqrt{\frac{U_0}{2\nu L}}e^{(x+y/2L)}z.
\end{aligned} \tag{12}$$

Equation (3) is identically satisfied and Equations (4)–(8) and (11) take the following forms:

$$\left(1+\frac{1}{\beta}\right)f'''-2(f'+g')f'+(f+g)f''+\lambda(\theta+Nr\phi)+\frac{M}{(\alpha_e^2+\beta_e^2)}(\beta_e g'-\alpha_e f')=0, \tag{13}$$

$$\left(1+\frac{1}{\beta}\right)g'''-2(f'+g')g'+(f+g)g''-\frac{M}{(\alpha_e^2+\beta_e^2)}\cdot(\beta_e f'+\alpha_e g')=0, \tag{14}$$

$$\frac{1}{\Pr}\left(1+\frac{4}{3}R\right)\theta''+(f+g)\theta'-n(f'+g')\theta+Nb\theta'\phi'+Nt\theta'^2+Q\theta=0, \tag{15}$$

$$\phi''-\mathrm{Sc}.n(f'+g')\phi+\mathrm{Sc}(f+g)\phi'+\frac{Nt}{Nb}\theta''=0, \tag{16}$$

$$\begin{aligned}
f(0)&=0,\\
f'(0)&=1,\\
g(0)&=0,\\
g'(0)&=c,\\
\theta(0)&=1,\\
\phi(0)&=1,\\
\text{for }\eta&=0,\\
f'&\longrightarrow 0,\\
g'&\longrightarrow 0,\\
\theta&\longrightarrow 0,\\
\phi&\longrightarrow 0,\\
\text{as }\eta&\longrightarrow\infty,
\end{aligned} \tag{17}$$

where $M=2L\sigma B_0^2/\rho U_w$, $\alpha_e=1+\beta_e\beta_i$, $\Pr=\upsilon/\alpha$, $R=(4\sigma^* T_\infty^3/\kappa^*\kappa)$, $Nb=\tau D_B(C_w-C_\infty)/\upsilon$.

The skin friction coefficients C_{fx} and C_{fy}, the local Nusselt number Nu_x, and Sherwood number Sh_x are defined as follows:

$$\begin{aligned}
C_{fx}&=\frac{2\tau_{wx}}{\rho U_w^2},\\
C_{fy}&=\frac{2\tau_{wy}}{\rho V_w^2},\\
Nu_x&=\frac{xq_w}{k(T_W-T_\infty)},\\
Sh_x&=\frac{xj_m}{D_B(C_W-C_\infty)},
\end{aligned} \tag{18}$$

where τ_{wx} and τ_{wy} are the wall shear stress along the $x-$ and $y-$ directions, respectively, q_w is the wall heat flux and j_w is the wall mass flux. These are as under:

$$\begin{aligned}
\tau_{wx}&=\mu\left(1+\frac{1}{\beta}\right)\left(\frac{\partial u}{\partial z}\right)\Big|_{z=0},\\
\tau_{wy}&=\mu\left(1+\frac{1}{\beta}\right)\left(\frac{\partial v}{\partial z}\right)\Big|_{z=0},\\
q_w&=-k\left(1+\frac{4}{3}R\right)\left(\frac{\partial T}{\partial z}\right)\Big|_{z=0},\\
j_w&=-D_B\left(\frac{\partial C}{\partial z}\right)\Big|_{z=0}.
\end{aligned} \tag{19}$$

From equations (12) and (18) and (19), we obtain

$$C_{fx}\sqrt{\frac{\mathrm{Re}_x}{2}} = \left(1+\frac{1}{\beta}\right)f''(0),$$
$$C_{fy}\sqrt{\frac{\mathrm{Re}_y}{2}} = \left(1+\frac{1}{\beta}\right)g''(0),$$
$$\frac{Nu_x}{\sqrt{\mathrm{Re}_x}} = -\left(1+\frac{4}{3}R\right)\theta'(0), \quad (20)$$
$$\frac{Sh_x}{\sqrt{\mathrm{Re}_x}} = -\phi'(0),$$

where $\mathrm{Re}_x = U_w L/\nu$ and $\mathrm{Re}_y = V_w L/\nu$.

3. Method of Solution

Equations (13)–(16) depending on the boundary conditions (17) are solved employing the spectral relaxation method [42, 45–50]. This method is chosen as it has been exposed to be accurate and in general easier to employ compared to other ordinary numerical methods, for instance finite difference method. The spectral relaxation algorithm utilizes the notion of Gauss–Seidel method to decouple the system of governing Equations (13)–(16). The method is developed by evaluating the linear terms at the present iteration level $r+1$ and nonlinear terms at the preceding iteration level r. The Chebyshev pseudospectral strategy is utilized to solve the decoupled equations. In this method, we present a differentiation matrix D which is roughly the derivative of the unknown variables, for instance, $f(\eta)$ at collocation points as the matrix vector product is

$$\frac{\mathrm{d}f}{\mathrm{d}\eta} = \sum_{k=0}^{N} \mathbf{D}_{jk} f(\zeta_k) = \mathbf{Df}, \quad j = 0, 1, 2, \ldots, N, \quad (21)$$

where $N+1$ is the number of collocation points (or grid points), $\mathbf{D} = 2D/\eta_\infty$, and $\mathbf{f} = [f(\zeta_0)\ \ f(\zeta_1)\ \ \ldots\ \ f(\zeta_N)]^T$ is the vector function at the collocation points. η_∞ is a finite length which is sufficiently large so that we can easily include the condition at infinity in this point. A variable ζ is used to map the truncated interval $[0, \eta_\infty]$ to the interval $[-1, 1]$ on which the spectral method can be executed.

The algorithm for the SRM may be summarized as follows:

(1) Introduce the transformation $f'(\eta) = p(\eta)$ and convey the original equation in terms of $p(\eta)$ to reduce the order of the momentum equation (13) for $f(\eta)$.

(2) Assuming that $f(\eta)$ is identified from a prior iteration (denoted by f_r), make an iteration scheme for $p(\eta)$ by assuming that only linear terms in $p(\eta)$ are to be calculated at the recent iteration level (denoted by p_{r+1}), and all other linear and nonlinear terms are understood to be known from the prior iteration. Besides, nonlinear terms in p are calculated at the prior iteration.

(3) Introduce the transformation $g'(\eta) = h(\eta)$ and convey the original equation in terms of $h(\eta)$ to reduce the order of the momentum equation (14) for $g(\eta)$.

(4) Assuming that $g(\eta)$ is identified from a prior iteration (denoted by g_r), make an iteration scheme for $h(\eta)$ by assuming that only linear terms in $h(\eta)$ are to be calculated at the recent iteration level (denoted by h_{r+1}) and all other linear and nonlinear terms are understood to be known from the prior iteration. Besides, nonlinear terms in h are calculated at the prior iteration.

(5) The iteration schemes for the remaining governing dependent variables are developed correspondingly but at the present using the updated solutions of the variables determined in the preceding equation.

(6) Chose suitable initial guesses which satisfy the given boundary conditions.

Thus, to employ the SRM, we begin by reducing the order of the momentum, equations (13) and (14), from third to second order introducing the transformation $f' = p$ and $g' = h$ so that $f'' = p'$, $f''' = p''$, $g'' = h'$, and $g''' = h''$. Thus, equations (13)–(16) become

$$f' = p, \quad (22)$$

$$\left(1+\frac{1}{\beta}\right)p'' + (f+g)p' - \left(2h + \frac{M\alpha_e}{\left(\alpha_e^2+\beta_e^2\right)}\right)p = 2p^2 - \lambda(\theta + Nr\phi) - \frac{M\beta_e}{\left(\alpha_e^2+\beta_e^2\right)}h, \quad (23)$$

$$g' = h, \quad (24)$$

$$\left(1+\frac{1}{\beta}\right)h'' + (f+g)h' - \left(2p + \frac{M\alpha_e}{\left(\alpha_e^2+\beta_e^2\right)}\right)h = 2h^2 + \frac{M\beta_e}{\left(\alpha_e^2+\beta_e^2\right)}p, \quad (25)$$

$$\frac{1}{\mathrm{Pr}}\left(1+\frac{4}{3}R\right)\theta'' + (f+g+Nb\phi')\theta' - n\left(p+h+\frac{Q}{n}\right)\theta = -Nt\theta'^2, \quad (26)$$

$$\phi'' + \mathrm{Sc}(f+g)\phi' - \mathrm{Sc}.n(p+h)\phi = -\frac{Nt}{Nb}\theta'', \quad (27)$$

and the boundary conditions are written as

$$\begin{aligned} f(0) &= 0, \\ p(0) &= 1, \\ g(0) &= 0, \\ h(0) &= c, \\ \theta(0) &= 1, \\ \phi(0) &= 1, \\ \text{for } \eta &= 0, \\ p &\longrightarrow 0, \\ h &\longrightarrow 0, \\ \theta &\longrightarrow 0, \\ \phi &\longrightarrow 0, \\ \text{as } \eta &\longrightarrow \infty. \end{aligned} \quad (28)$$

Implementing the SRM to equations (22)–(27), we get the subsequent iteration scheme:

$$\left(1+\frac{1}{\beta}\right)p''_{r+1}+(f_r+g_r)p'_{r+1}-\left(2h_r+\frac{M\alpha_e}{\left(\alpha_e^2+\beta_e^2\right)}\right)p_{r+1}$$
$$=2p_r^2-\lambda(\theta_r+Nr\phi_r)-\frac{M\beta_e}{\left(\alpha_e^2+\beta_e^2\right)}h_r,$$

$$f_{r+1}'=p_{r+1},$$

$$\left(1+\frac{1}{\beta}\right)h''_{r+1}+(f_{r+1}+g_r)h'_{r+1}-\left(2p_{r+1}+\frac{M\alpha_e}{\left(\alpha_e^2+\beta_e^2\right)}\right)h_{r+1}$$
$$=2h_r^2+\frac{M\beta_e}{\left(\alpha_e^2+\beta_e^2\right)}p_{r+1},$$

$$g'_{r+1}=h_{r+1},$$

$$\frac{1}{\Pr}\left(1+\frac{4}{3}R\right)\theta''_{r+1}+(f_{r+1}+g_{r+1}+Nb\phi_r')\theta'_{r+1}-n\cdot(p_{r+1}+h_{r+1}+Q/n)\theta_{r+1}$$

$$\phi''_{r+1}+\mathrm{Sc}(f_{r+1}+g_{r+1})\phi'_{r+1}-\mathrm{Sc}.n(p_{r+1}+h_{r+1})\phi_{r+1}$$
$$=-\frac{Nt}{Nb}\theta''_{r+1},$$

(29)

and the boundary conditions are written as

$$\begin{aligned}
f_{r+1}(0)&=0,\\
p_{r+1}(0)&=1,\\
g_{r+1}(0)&=0,\\
h_{r+1}(0)&=c,\\
\theta_{r+1}(0)&=1,\\
\phi_{r+1}(0)&=1,\\
\text{for }\eta&=0,\\
p_{r+1}&\longrightarrow 0,\\
h_{r+1}&\longrightarrow 0,\\
\theta_{r+1}&\longrightarrow 0,\\
\phi_{r+1}&\longrightarrow 0,\\
\text{as }\eta&\longrightarrow\infty.
\end{aligned}\tag{30}$$

The system of the equations along with the boundary conditions are written in a matrix form as

$$\begin{aligned}
\mathbf{A}_1\mathbf{p}_{\mathbf{r}+1}&=\mathbf{B}_1,\\
p_{r+1}(\zeta_N)&=1,\\
p_{r+1}(\zeta_0)&=0,
\end{aligned}\tag{31}$$

$$\begin{aligned}
\mathbf{A}_2\mathbf{f}_{\mathbf{r}+1}&=\mathbf{B}_2,\\
f_{r+1}(\zeta_N)&=0,
\end{aligned}\tag{32}$$

$$\begin{aligned}
\mathbf{A}_3\mathbf{h}_{\mathbf{r}+1}&=\mathbf{B}_3,\\
h_{r+1}(\zeta_N)&=c,\\
h_{r+1}(\zeta_0)&=0,
\end{aligned}\tag{33}$$

$$\begin{aligned}
\mathbf{A}_4\mathbf{g}_{\mathbf{r}+1}&=\mathbf{B}_4,\\
g_{r+1}(\zeta_N)&=0,
\end{aligned}\tag{34}$$

$$\begin{aligned}
\mathbf{A}_5\boldsymbol{\theta}_{\mathbf{r}+1}&=\mathbf{B}_5,\\
\theta_{r+1}(\zeta_N)&=1,\\
\theta_{r+1}(\zeta_0)&=0,
\end{aligned}\tag{35}$$

$$\begin{aligned}
\mathbf{A}_6\boldsymbol{\phi}_{\mathbf{r}+1}&=\mathbf{B}_6,\\
\phi_{r+1}(\zeta_N)&=1,\\
\phi_{r+1}(\zeta_0)&=0,
\end{aligned}\tag{36}$$

and the matrices are defined as

$$\mathbf{A}_1=\left(1+\frac{1}{\beta}\right)\mathbf{D}^2+\mathrm{diag}(f_r+g_r)\mathbf{D}-\left(2h_r+\frac{M\alpha_e}{\left(\alpha_e^2+\beta_e^2\right)}\right)\mathbf{I},$$

$$\mathbf{B}_1=2p_r^2-\lambda(\theta_r+Nr\phi_r)-\frac{M\beta_e}{\left(\alpha_e^2+\beta_e^2\right)}h_r,$$

$$\mathbf{A}_2=\mathbf{D},$$

$$\mathbf{B}_2=p_{r+1},$$

$$\mathbf{A}_3=\left(1+\frac{1}{\beta}\right)\mathbf{D}^2+\mathrm{diag}(f_{r+1}+g_r)\mathbf{D}-\left(2p_{r+1}+\frac{M\alpha_e}{\left(\alpha_e^2+\beta_e^2\right)}\right)\mathbf{I},$$

$$\mathbf{B}_3=2h_r^2+\frac{M\beta_e}{\left(\alpha_e^2+\beta_e^2\right)}p_{r+1},$$

$$\mathbf{A}_4=\mathbf{D},$$

$$\mathbf{B}_4=h_{r+1},$$

$$\mathbf{A}_5=\frac{1}{Pr}\left(1+\frac{4}{3}R\right)\mathbf{D}^2+\mathrm{diag}(f_{r+1}+g_{r+1}+Nb\phi_r')\mathbf{D}-n(p_{r+1}+h_{r+1}+Q/A)\mathbf{I},$$

$$\mathbf{B}_5=-Nt\theta_r^{'2},$$

$$\mathbf{A}_6=\mathbf{D}^2+\mathbf{Sc}(f_{r+1}+g_{r+1})\mathbf{D}-\mathrm{Sc}.n(p_{r+1}+h_{r+1})\mathbf{I},$$

$$\mathbf{B}_6=-\frac{Nt}{Nb}\theta''_{r+1},$$

(37)

where $\mathbf{I}$ and diag $[\cdot]$ are the identity and diagonal matrices of order $(N+1)\times(N+1)$, respectively, and $\mathbf{f}, \mathbf{p}, \mathbf{g}, \mathbf{h}, \boldsymbol{\theta}$, and $\boldsymbol{\phi}$ are, respectively, the values of f, p, g, h, θ, and ϕ, when

evaluated at the collocation (or grid) points. equations (31)–(36) constitute the SRM scheme. Since they are decoupled, they may be solved separately. This is preceded by applying boundary conditions as shown follows:

$$\begin{pmatrix} 1\,0\ldots 0 \\ A_1 \\ 0\ldots 0\,1 \end{pmatrix}\begin{pmatrix} p_{r+1}(\xi_0) \\ \vdots \\ p_{r+1}(\xi_N) \end{pmatrix} = \begin{pmatrix} 0 \\ B_1 \\ 1 \end{pmatrix},$$

$$\begin{pmatrix} A_2 \\ 0\ldots 0\,1 \end{pmatrix}\begin{pmatrix} f_{r+1}(\xi_0) \\ \vdots \\ f_{r+1}(\xi_N) \end{pmatrix} = \begin{pmatrix} B_2 \\ 0 \end{pmatrix},$$

$$\begin{pmatrix} 1\,0\ldots 0 \\ A_3 \\ 0\ldots 0\,1 \end{pmatrix}\begin{pmatrix} h_{r+1}(\xi_0) \\ \vdots \\ h_{r+1}(\xi_N) \end{pmatrix} = \begin{pmatrix} 0 \\ B_3 \\ c \end{pmatrix},$$

$$\begin{pmatrix} A_4 \\ 0\ldots 0\,1 \end{pmatrix}\begin{pmatrix} g_{r+1}(\xi_0) \\ \vdots \\ g_{r+1}(\xi_N) \end{pmatrix} = \begin{pmatrix} B_4 \\ 0 \end{pmatrix}, \quad (38)$$

$$\begin{pmatrix} 1\,0\ldots 0 \\ A_5 \\ 0\ldots 0\,1 \end{pmatrix}\begin{pmatrix} \theta_{r+1}(\xi_0) \\ \vdots \\ \theta_{r+1}(\xi_N) \end{pmatrix} = \begin{pmatrix} 0 \\ B_5 \\ 1 \end{pmatrix},$$

$$\begin{pmatrix} 1\,0\ldots 0 \\ A_6 \\ 0\ldots 0\,1 \end{pmatrix}\begin{pmatrix} \phi_{r+1}(\xi_0) \\ \vdots \\ \phi_{r+1}(\xi_N) \end{pmatrix} = \begin{pmatrix} 0 \\ B_6 \\ 1 \end{pmatrix}.$$

Selected initial guesses that gratify the given boundary conditions (17) are

$$\begin{aligned} f_0(\eta) &= 1 - e^{-\eta}, \\ p_0(\eta) &= e^{-\eta}, \\ g_0(\eta) &= c\left(1 - e^{-\eta}\right), \\ h_0(\eta) &= ce^{-\eta}, \\ \theta_0(\eta) &= \phi_0(\eta) = e^{-\eta}. \end{aligned} \quad (39)$$

4. Results and Discussions

Equations (13)–(16) subject to the boundary conditions (17) are solved numerically employing SRM. The numerical solutions for the given flow problem are obtained for velocities, thermal and concentration distributions, skin friction coefficients, local Nusselt, and Sherwood numbers for different values of physical parameters through graphs shown in Figures 2–18. Unless otherwise stated, the default numerical values for the parameters are taken to be fixed as $\beta = \lambda = Nb = Nt = c = 0.5, M = 3.0, \beta_e = \beta_i = 2.0, Nr = Q = 1.0, \mathrm{Pr} = 10, R = n = 2.0$, and $\mathrm{Sc} = 5.0$. The ranges of parameters used in Figures 2–18 are $0.4 \le \beta \le 1.0$, $2.0 \le M \le 6.0, 1.0 \le \beta_e \le 6.0, 1.0 \le \beta_i \le 6.0, 0.1 \le \lambda \le 1.0$, $10 \le Pr \le 20, 1.0 \le R \le 3.0, 0.4 \le c \le 0.8, 0.2 \le Nb \le 0.6, 0.5 \le Nt \le 1.5$, $2.0 \le n \le 4.0, 3.0 \le Sc \le 6.0, 0.0 \le Nr \le 10.0$, and $0.0 \le Q \le 1.0$.

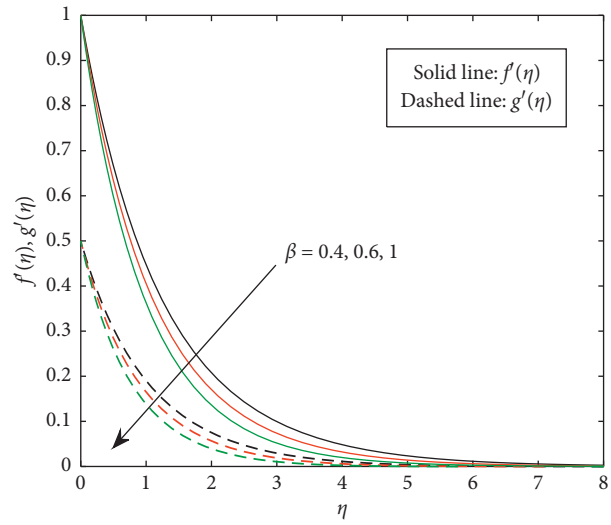

Figure 2: Influence of β on $f'(\eta)$ and $g'(\eta)$.

The numerical values for the physical parameters are calculated in the chosen interval in an attempt to understand the flow behavior in a better way and to be sufficient in providing accurate solution.

For the substantiation of the numerical method used, the results are compared with the previously obtained results for various values of parameters, and it indicates an excellent agreement as depicted in Tables 1 and 2.

Figure 2 shows the impact of Casson fluid parameter (β) on the velocity distributions $f'(\eta)$ and $g'(\eta)$. An expansion in Casson fluid parameter (β) leads to a decrease in the yield stress and momentum boundary layer thickness. Owing to this fact, velocity distributions reduce with an increment in the values of β. Physically, the fluid turns out to be more viscous with mounting Casson fluid parameter (β). Figure 3 outlines the impact of magnetic parameter M on the velocity profiles $f'(\eta)$ and $g'(\eta)$. As the value of M expands, velocity diminishes because of Lorentz forces which slow down the velocity of the fluid. Along these lines both boundary layer thickness and the magnitude of the velocity profiles $f'(\eta)$ and $g'(\eta)$ diminish. The impact of Hall parameter (β_e) on velocity profiles $f'(\eta)$ and $g'(\eta)$ is shown in Figure 4. It is noticed that velocity profiles $f'(\eta)$ and $g'(\eta)$ have expanding tendency when Hall parameter (β_e) is expanded. Moreover, the momentum boundary layer thickness is expanded by expanding the Hall parameter (β_e). This is because of the fact that magnetic field and Lorentz force decline when Hall parameter is expanded.

The impact of ion slip parameter (β_i) on the velocity profiles $f'(\eta)$ and $g'(\eta)$ is shown in Figure 5. It is clear from Figure 5 that both boundary layer thickness and the magnitude of the velocity profiles $f'(\eta)$ and $g'(\eta)$ increment when ion slip parameter is expanded in light of the fact that magnetic field impacts because ion slip is inverse to applied magnetic field. This opposes the impacts of Lorentz force because of the applied magnetic field. It implies Lorentz force diminishes when ion slip parameter is expanded and therefore $f'(\eta)$ and $g'(\eta)$ increment when ion slip parameter (β_i) is expanded. Figure 6 exhibits the impact of the mixed

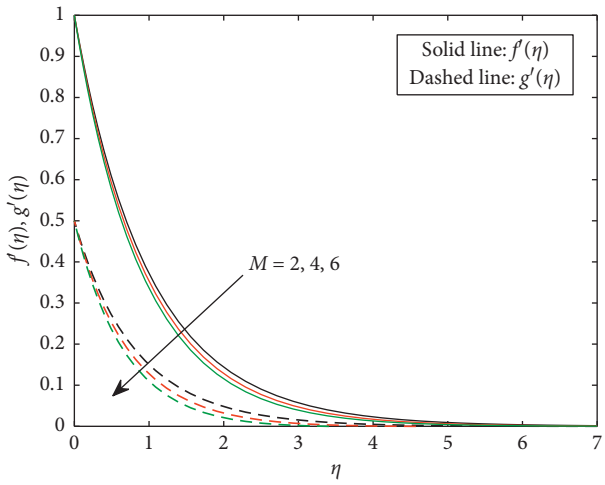

Figure 3: Influence of M on $f'(\eta)$ and $g'(\eta)$.

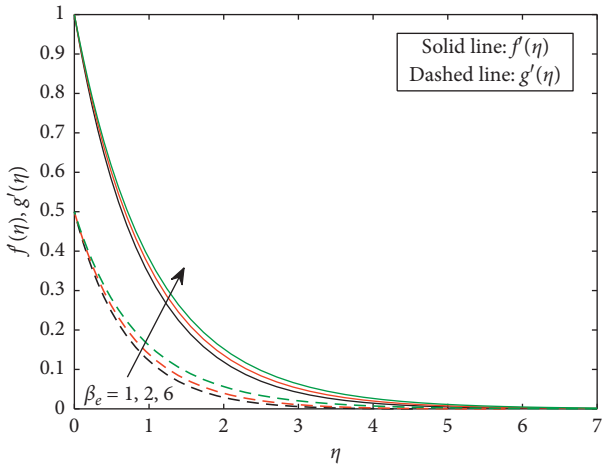

Figure 4: Influence of β_e on $f'(\eta)$ and $g'(\eta)$.

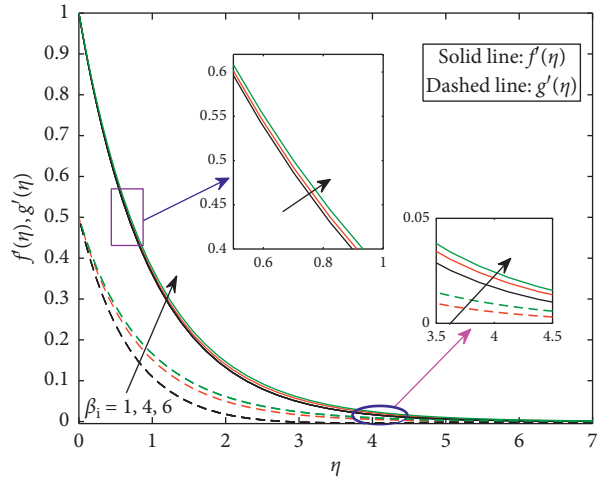

Figure 5: Influence of β_i on $f'(\eta)$ and $g'(\eta)$.

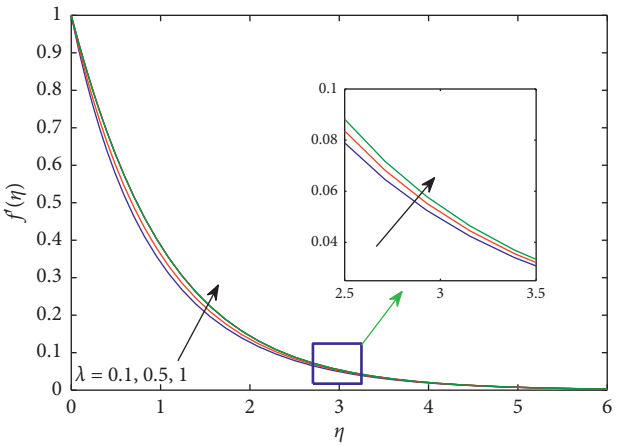

Figure 6: Influence of λ on $f'(\eta)$.

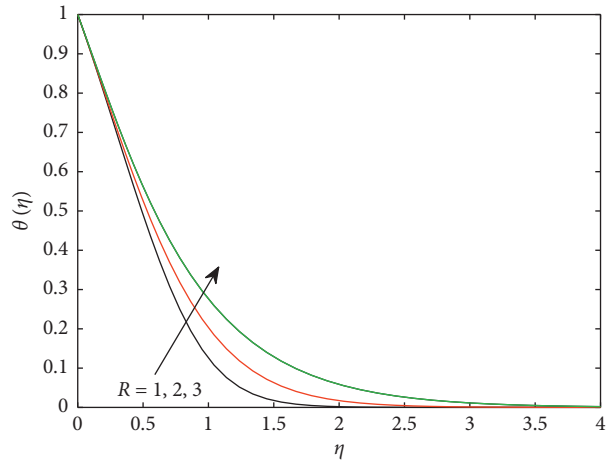

Figure 7: Influence of R on $\theta(\eta)$.

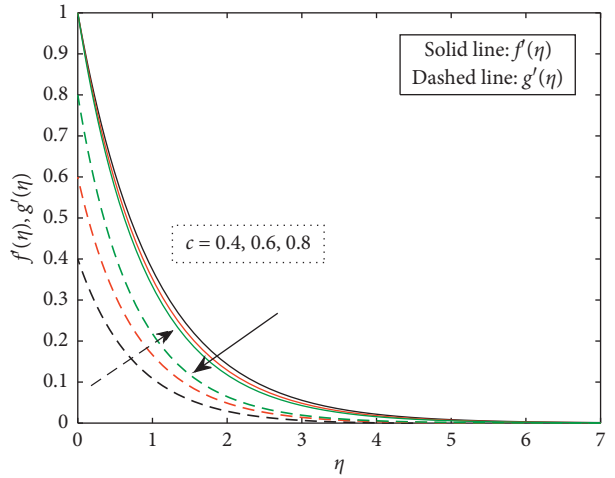

Figure 8: Influence of c on $f'(\eta)$ and $g'(\eta)$.

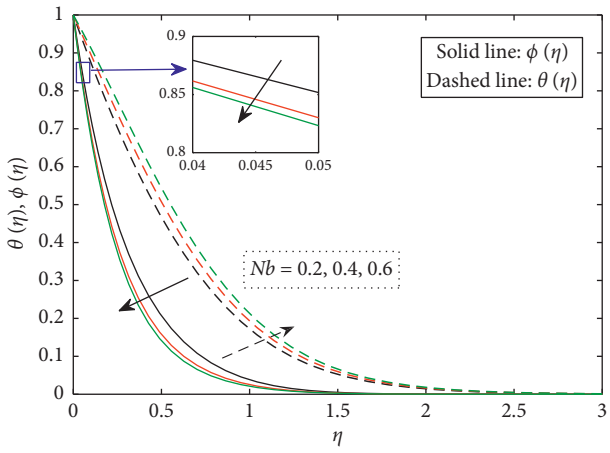

Figure 9: Influence of Nb on $\theta(\eta)$ and $\phi(\eta)$.

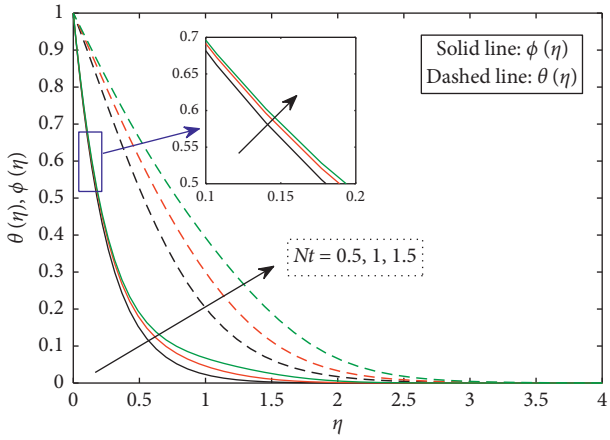

Figure 10: Influence of Nt on $\theta(\eta)$ and $\phi(\eta)$.

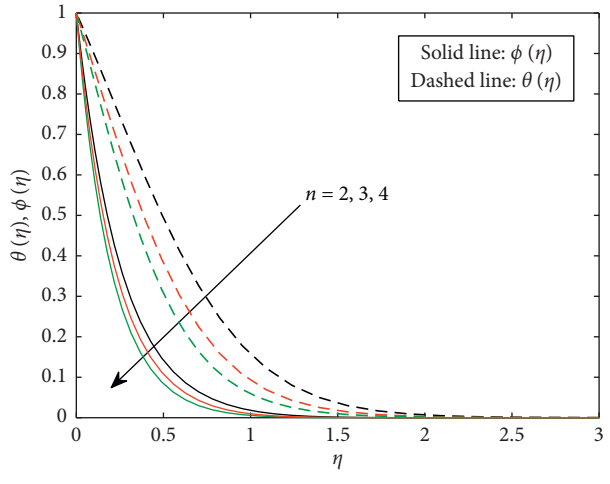

Figure 11: Influence of n on $\theta(\eta)$ and $\phi(\eta)$.

convection parameter (λ) on the velocity profile $f'(\eta)$. It is seen that the velocity distribution increments as the value of λ rises because of buoyancy impact. Figure 7 uncovers the

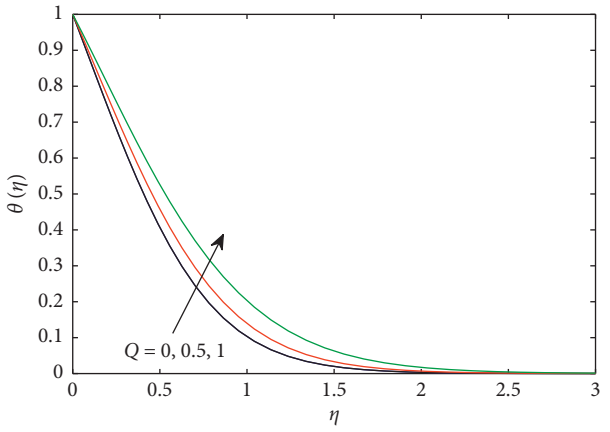

Figure 12: Influence of Q on $\theta(\eta)$.

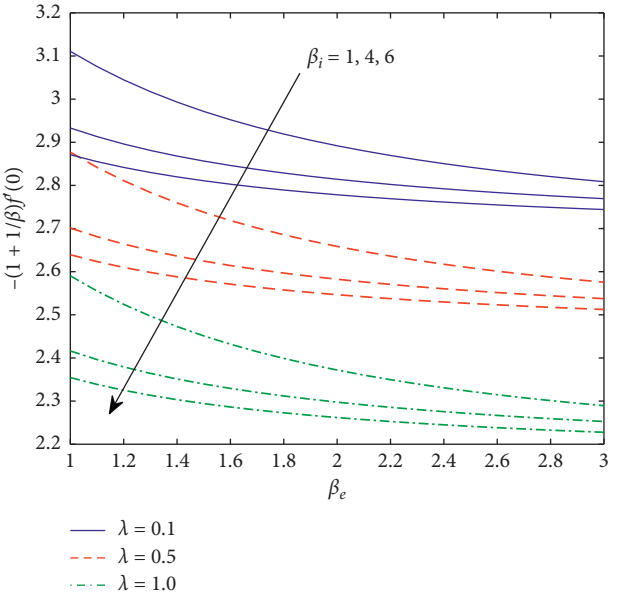

Figure 13: Influence of β_e, β_i, and λ on the skin friction coefficient $-(1 + (1/\beta))f''(0)$.

alterations that are seen in nanofluid temperature profiles because of increment in the values of radiation parameter (R). It merits seeing that the nanofluid temperature increments as thermal radiation increment because of the way that the conduction effect of the nanofluid improves within the sight of thermal radiation. Henceforth, higher values of radiation parameter imply higher surface heat flux and thus upgrade the temperature inside the boundary layer area. Figure 8 portrays the impact of velocity ratio parameter (c) on $f'(\eta)$ and $g'(\eta)$. An expansion in ratio parameter (c) diminishes the boundary layer thickness for $f'(\eta)$ and increments $g'(\eta)$. Physically, when c enhances, the stretching rate augments in the y–direction. Subsequently, the velocity amplifies in the y–direction. Here, $c = 0$ denotes two-dimensional cases. In the event that $c = 1$, the characteristics of the stream along both directions are alike.

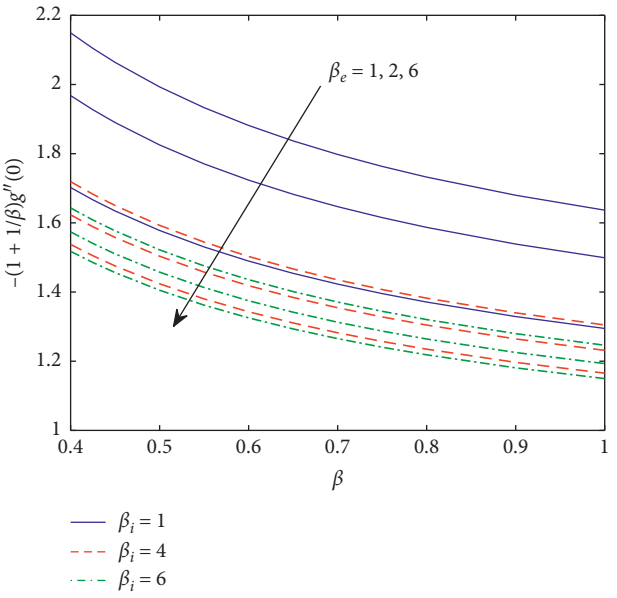

Figure 14: Influence of β, β_e, and β_i on the skin friction coefficient $-(1 + (1/\beta))g''(0)$.

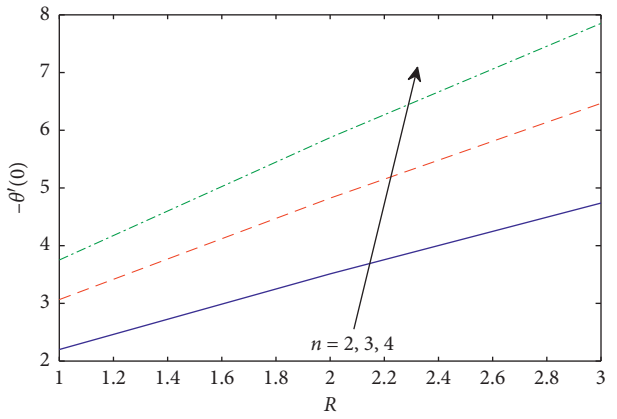

Figure 15: Influence of n and R on the local Nusselt number $-\theta'(0)$.

The impact of Brownian motion parameter (Nb) on temperature $\theta(\eta)$ and concentration $\phi(\eta)$ is exhibited in Figure 9. Brownian motion is the arbitrary movement of small colloidal particles suspended in a fluid, brought about by the collision of the fluid atoms with the particles. An improvement in the Brownian motion yields noteworthy movement of the nanoparticles that offers an increment in the fluid kinetic energy, and as a result the fluid temperature increases. In addition, thermal boundary layer thickens when Nb is expanded. In contrast, it is seen that the concentration $\phi(\eta)$ and related boundary layer thickness lessens with an improvement in Nb. Figure 10 explains the impact of thermophoresis parameter (Nt) on the temperature $\theta(\eta)$ and nanoparticle volume fraction $\phi(\eta)$. Escalating values of Nt shows stronger thermophoretic force because of temperature gradient which moves the nanoparticles from the

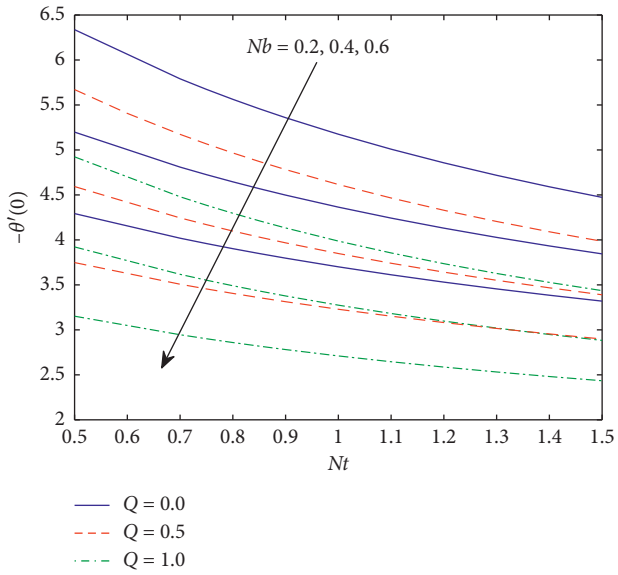

Figure 16: Influence of Nb, Nt, and Q on the local Nusselt number $-\theta'(0)$.

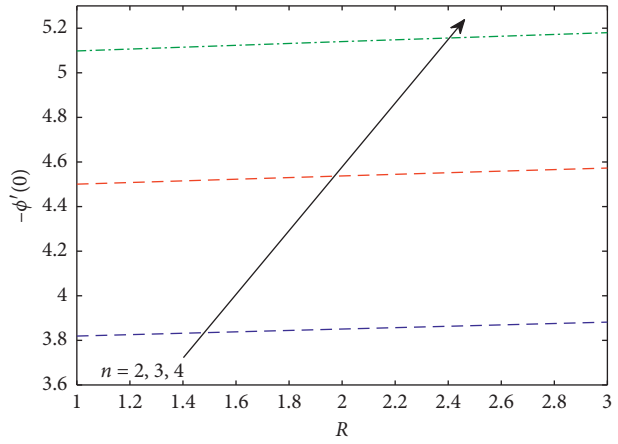

Figure 17: The influence of n and R on the local Sherwood number, $-\phi'(0)$.

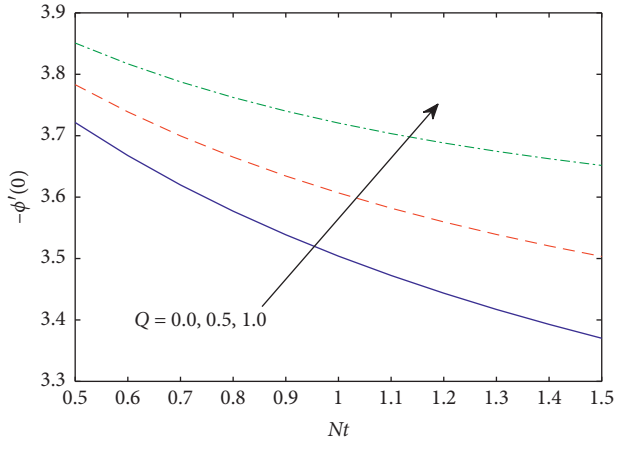

Figure 18: The influence of Nt and Q on the local Sherwood number, $-\phi'(0)$.

Table 1: Comparison of $-f'(0)$ and $-g'(0)$ for different values of c when $M = \lambda = 0$ and $\beta = \infty$.

	Liu et al. [44]		Hayat et al. [51]		Present results	
c	$-f''(0)$	$-g''(0)$	$-f''(0)$	$-g''(0)$	$-f''(0)$	$-g''(0)$
0.5	1.56988846	0.78494423	1.569889	0.784944	1.5698884578	0.7849442289
1.0	1.81275105	1.81275105	1.812751	1.812751	1.8127510474	1.8127510474

Table 2: Comparison of $-\theta,(0)$ in case of ordinary fluids ($Nb = Nt = 10^{-9}$) for different values of c, Pr, and n when $M = \lambda = 0$ and $\beta = \infty$.

c	Pr	n	Liu et al. [44]	Khan et al. [4]	Rao et al. [45]	Present results
0.5	0.7	−2	−0.76378454	−0.76367407	−0.7637932240	−0.7637845438
		0	0.52154103	0.52152683	0.5215376637	0.5215410326
		5	2.01061361	2.0102735	2.0106070569	2.0106136104
	7	−2	−7.27614126	−7.2596204	−7.2763849638	−7.2761413999
		0	2.26162085	2.2631841	2.2616092689	2.2616208431
		5	7.22330493	7.2229124	7.2232801587	7.2233049205
1	0.7	−2	−0.88194314	−0.88177213	−0.8819517699	−0.8819431406
		0	0.60222359	0.6022019	0.6022200405	0.6022235865
		5	2.32165661	2.3211331	2.3216491323	2.3216566118
	7	−2	−8.40176423	−8.3764364	−8.4020449202	−8.4017643908
		0	2.61149481	2.6139021	2.6114815046	2.6114948052
		5	8.34075409	8.3401528	8.3407255264	8.3407540806

hot sheet to the quiescent fluid accordingly mounting the temperature and nanoparticle volume fraction boundary layer.

Figure 11 indicates that an augment in temperature exponent parameter (n) caused a decrease in both temperature and concentration profiles. Besides, the thermal and concentration boundary layer thickness lessen with increment in temperature exponent parameter (n). Figure 12 explains the impact of heat source parameter (Q) on the temperature distribution $\theta(\eta)$. Overall, heat generation parameter in the fluid expands the temperature. Accordingly, an expansion in Q upgrades the temperature and thermal boundary layer thickness.

Figure 13 demonstrates the skin friction coefficient $-(1 + (1/\beta))f''(0)$ for different values of ion slip parameter (β_i)and mixed convection parameter (λ). The skin friction coefficient $-(1 + (1/\beta))f''(0)$ is a decreasing function of Hall parameter (β_e). Moreover, the increase in β_i and λ decreases the skin friction coefficient $-(1 + (1/\beta))f''(0)$. Similarly, the skin friction coefficient $-(1 + (1/\beta))g''(0)$ is a diminishing function of Casson fluid parameter (β) and the augment in β_e and β_i reduces the skin friction coefficient $-(1 + (1/\beta))g''(0)$ as shown in Figure 14. Furthermore, Figure 15 depicts that the local Nusselt number $-\theta'(0)$ is an escalating function of radiation parameter (R), and the rise in temperature exponent parameter (n) enhances the local Nusselt number $-\theta'(0)$. On the contrary, Figure 16 shows that the local Nusselt number $-\theta\prime(0)$ is a declining function of thermophoresis parameter (Nt), and the increase in Brownian motion parameter (Nb) and heat source parameter (Q) decreases the local Nusselt number $-\theta'(0)$. Moreover, Figure 17 represents that the local Sherwood number $-\phi'(0)$ is an increasing function of radiation parameter (R), and the increase in temperature exponent parameter (n) amplifies the local Sherwood number $-\phi'(0)$. In contrast, the local Sherwood number $-\phi'(0)$ is a decreasing function of thermophoresis parameter (Nt), and the augment in heat source parameter Q boosts the local Sherwood number $-\phi'(0)$ as depicted in Figure 18.

5. Conclusions

A numerical study of three-dimensional MHD mixed convection flow of Casson nanofluid over an exponentially stretching sheet with Hall and ion slip effects has been investigated. The numerical solutions for the considered flow problem are obtained employing spectral relaxation method (SRM). The impacts of different significant parameters on the velocities, temperature, and nanoparticle concentration distributions have been considered graphically. Moreover, the numerical results for the skin friction coefficients, local Nusselt, and Sherwood numbers have been presented graphically. Accordingly, the major results of the present study are

(a) The velocity profiles along both $x-$ and $y-$directions enhance with an increment in the Hall parameter (β_e) and ion slip parameter (β_i) while the opposite inclination is observed with a rise in Casson fluid parameter (β) and magnetic field parameter (M).

(b) The velocity distribution along $x-$direction boosts with a rise in mixed convection parameter (λ).

(c) The temperature profile enhances with increasing values of the Brownian motion parameter (Nb), thermophoresis parameter (Nt), thermal radiation parameter (R), and heat source parameter (Q), and it

declines for increasing values of stretching ratio parameter (c) and temperature exponent parameter (n).

(d) The concentration distribution rises with an increment in the thermophoresis parameter (Nt) and it diminishes as the Brownian motion parameter (Nb), stretching ratio parameter (c), and temperature exponent parameter (n) enlarge.

(e) Both the skin friction coefficients reduce as Casson fluid parameter (β), Hall parameter (β_e), and ion slip parameter (β_i) rise.

(f) Both the local Nusselt and Sherwood numbers are increasing functions of the thermal radiation parameter (R) and temperature exponent parameter (n). Moreover, opposite conditions are noticed for the local Nusselt and Sherwood numbers as Brownian motion parameter (Nb) and heat source parameter (Q) increase.

5.1. Recommendations. It is important to emphasize few limitations about this research work. Such limitations will help researchers to analyze and provide an extension of the present work. Thus, the following assumptions and limitations can be considered:

(i) The same problem can be calculated under the deliberation of different nanoparticles, viscous dissipation, ohmic heating, Newtonian heating, etc.

(ii) To extend present results using convective boundary condition or/and slip condition.

Nomenclature

x, y, z: Cartesian coordinates
u, v, w: Velocity components
U_w, V_w: Velocities of the stretching sheet
B_0: Constant magnetic field
g: Acceleration due to gravity
T: Fluid temperature
T_w: Surface temperature
T_∞: Ambient temperature
C: Concentration of fluid
C_w: Surface concentration
C_∞: Ambient concentration
M: Magnetic field parameter
Gr_x: Local grashof number
Re_x: Local reynolds number
Nr: Buoyancy ratio
Pr: Prandtl number
D_B: Brownian diffusion coefficient
D_T: Thermophoresis diffusion coefficient
Nb: Brownian motion parameter
Nt: Thermophoresis parameter
Sc: Schmidt number
C_{fx}: Skin friction coefficient in $x-$direction
C_{fy}: Skin friction coefficient in $y-$direction
Nu_x: Local nusselt number
Sh_x: Local sherwood number
c: Velocity ratio parameter
L: Reference length
N: Temperature exponent parameter
R: Radiation parameter
Q_0: The dimensional heat generation
Q: Heat source parameter
f, g: Dimensionless stream functions

Greek letters

ρ: Density of fluid
v: Kinematic viscosity of the fluid
β: Casson fluid parameter
λ: Mixed convection parameter
α: Thermal diffusivity
κ: Thermal conductivity
σ: Electrical conductivity
β_e: Hall parameter
β_i: Ion slip parameter
β_t: Coefficient of thermal expansion
β_c: Coefficient of concentration expansion
η: Dimensionless similarity variable
θ: Dimensionless temperature
ϕ: Dimensionless concentration
$(\rho C)_p$: Effective heat capacity of a nanoparticle
$(\rho C)_f$: Heat capacity of the fluid $\tau = (\rho C)_p/(\rho C)_f$

Subscripts

f: Fluid
p: Nanoparticle
w: Condition at the surface
∞: Ambient condition

Superscripts

$\prime$: Differentiation w. r. t. η

Data Availability

No data were generated or analyzed during the contact study.

Conflicts of Interest

The authors declare that they have no conflicts of interest.

References

[1] C. S. Reddy, N. Kishan, and B. Ch. Shekar, "MHD boundary layer flow and heat transfer of a nanofluid over a shrinking sheet with mass suction and chemical reaction," *Journal of Nanofluids*, vol. 4, pp. 1–10, 2015.

[2] D. Ramya, R. S. Raju, J. A. Rao, and A. J. Chamkha, "Effects of velocity and thermal wall slip on magnetohydrodynamics (MHD) boundary layer viscous flow and heat transfer of a nanofluid over a non-linearly-stretching sheet: a numerical study," *Propulsion and Power Research*, vol. 7, no. 2, pp. 182–195, 2018.

[3] Q. Zhao, H. Xu, and T. Fan, "Analysis of three-dimensional boundary-layer nanofluid flow and heat transfer over a

stretching surface by means of the homotopy analysis method," *Boundary Value Problems*, vol. 64, pp. 1–18, 2015.

[4] J. A. Khan, M. Mustafa, T. Hayat, M. Sheikholeslami, and A. Alsaedi, "Three-dimensional flow of nanofluid induced by an exponentially stretching sheet: an application to solar energy," *PLoS One*, vol. 10, no. 3, Article ID e0116603, 18 pages, 2015.

[5] T. Hayat, T. Muhammad, A. Alsaedi, and B. Ahmad, "Three-dimensional flow of nanofluid with Cattaneo-Christov double diffusion," *Results in Physics*, vol. 6, pp. 897–903, 2016.

[6] Z. Shah, M. Sheikholeslami, P. Kumam, M. Shutaywi, and P. Thounthong, "CFD simulation of water-based hybrid nanofluid inside a porous enclosure employing Lorentz forces," *IEEE Access*, vol. 7, pp. 177177–177186, 2019.

[7] Z. Shah, E. O. Alzahrani, A. Dawar, A. Ullah, and I. Khan, "Influence of Cattaneo-Christov model on Darcy-Forchheimer flow of Micropolar Ferrofluid over a stretching/shrinking sheet," *International Communications in Heat and Mass Transfer*, vol. 110, Article ID 104385, 2020.

[8] Z. Shah, A. Khan, W. Khan et al., "Micropolar gold blood nanofluid flow and radiative heat transfer between permeable channels," *Computer Methods and Programs in Biomedicine*, vol. 186, Article ID 105197, 2020.

[9] N. A. Alreshidi, Z. Shah, A. Dawar, P. Kumam, M. Shutaywi, and W. Watthayu, "Brownian motion and thermophoresis effects on MHD three dimensional nanofluid flow with slip conditions and Joule dissipation due to porous rotating disk," *Molecules*, vol. 25, no. 3, p. 729, 2020.

[10] M. Izadi, S. M. R. H. Pour, A. K. Yasuri, and A. J. Chamkha, "Mixed convection of a nanofluid in a three-dimensional channel: effect of opposed buoyancy force on hydrodynamic parameters, thermal parameters and entropy generation," *Journal of Thermal Analysis and Calorimetry*, vol. 2, p. 16, 2018.

[11] F. Selimefendigil and A. J. Chamkha, "Magnetohydrodynamics mixed convection in a power law nanofluid filled triangular cavity with an opening using Tiwari and Das' nanofluid model," *Journal of Thermal Analysis and Calorimetry*, vol. 1, p. 18, 2018.

[12] N. Shukla, P. Rana, O. A. Bég, B. Singh, and A. Kadir, "Homotopy study of magnetohydrodynamic mixed convection nanofluid multiple slip flow and heat transfer from a vertical cylinder with entropy generation," *Propulsion and Power Research*, vol. 8, no. 2, pp. 147–162, 2019.

[13] F. Selimefendigil and H. F. Oztop, "Mixed convection and entropy generation of nanofluid flow in a vented cavity under the influence of inclined magnetic field," *Microsystem Technologies*, vol. 25, no. 12, pp. 4427–4438, 2019.

[14] M. J. H. Munshi, N. Jahan, and G. Mostafa, "Mixed convection heat transfer of nanofluid in a lid-driven porous medium square enclosure with pairs of heat source-sinks," *American Journal of Engineering Research (AJER)*, vol. 8, no. 6, pp. 59–70, 2019.

[15] T. Hayat, M. Bilal Ashraf, S. Shehzad et al., "Mixed convection flow of Casson nanofluid over a stretching sheet with convectively heated chemical reaction and heat source/sink," *Journal of Applied Fluid Mechanics*, vol. 8, no. 4, pp. 803–813, 2015.

[16] A. Kamran, S. Hussain, M. Sagheer, and N. Akmal, "A numerical study of magnetohydrodynamics flow in Casson nanofluid combined with Joule heating and slip boundary conditions," *Results in Physics*, vol. 7, pp. 3037–3048, 2017.

[17] A. A. Afify, "The influence of slip boundary condition on Casson nanofluid flow over a stretching sheet in the presence of viscous dissipation and chemical reaction," *Mathematical Problems in Engineering*, vol. 2017, Article ID 3804751, 12 pages, 2017.

[18] K. Govardhan, G. Narender, and G. S. Sarma, "MHD mixed convection flow of Casson nanofluid past a stretching sheet in the presence of viscous dissipation, chemical reaction and heat source/sink," *International Journal of Nanoparticle Research (IJNR)*, vol. 2, no. 9, pp. 1–13, 2019.

[19] M. Trivedi, O. Otegbeye, Md. S. Ansari, and S. S. Motsa, "A paired quasi-linearization on magnetohydrodynamic flow and heat transfer of Casson nanofluid with Hall effects," *Journal of Applied and Computational Mechanics*, vol. 5, no. 5, pp. 849–860, 2019.

[20] K. Rafique, M. I. Anwar, and M. Misiran, "Numerical study on micropolar nanofluid flow over an inclined surface by means of keller-box," *Asian Journal of Probability and Statistics*, vol. 14, no. 4, pp. 1–21, 2019.

[21] K. Rafique, M. I. Anwar, M. Misiran et al., "Numerical study on micropolar nanofluid flow over an inclined surface by means of keller-box," *Asian Journal of Probability and Statistics*, vol. 7, no. 139, pp. 1–21, 2019.

[22] M. Hamid, M. Usman, Z. H. Khan, R. Ahmad, and W. Wang, "Dual solutions and stability analysis of flow and heat transfer of Casson fluid over a stretching sheet," *Physics Letters A*, vol. 383, no. 20, pp. 2400–2408, 2019.

[23] P. Kumam, Z. Shah, A. Dawar, H. U. Rasheed, and S. Islam, "Entropy generation in MHD radiative flow of CNTs Casson nanofluid in rotating channels with heat source/sink," *Mathematical Problems in Engineering*, vol. 2019, Article ID 9158093, 14 pages, 2019.

[24] Z. Shah, P. Kumam, and W. Deebani, "Radiative MHD Casson nanofluid flow with activation energy and chemical reaction over past nonlinearly stretching surface through entropy generation," *Scientific Reports*, vol. 10, no. 1, pp. 1–14, 2020.

[25] M. Nawaz, T. Hayat, and A. Alsaedi, "Mixed convection three-dimensional flow in the presence of Hall and ion-slip effects," *Journal of Heat Transfer*, vol. 135, pp. 1–8, 2013.

[26] M. Nawaz and T. Zubair, "Finite element study of three dimensional radiative nano-plasma flow subject to Hall and ion slip currents," *Results in Physics*, vol. 7, pp. 4111–4122, 2017.

[27] T. R. K. D. V. Prasad, T. L. Raju, and K. V. B. Rajakumar, "Influence of Hall and ion-slip current on span-wise-cosinusoidally fluctuating MHD free convective fluid flow past an inclined porous plate with chemical reaction and soret effect," *International Journal of Advanced Scientific Research and Management*, vol. 4, no. 4, pp. 118–125, 2019.

[28] S. Nasrin, M. R. Islam, and Md. M. Alam, "Hall and ion-slip current effect on steady MHD fluid flow along a vertical porous plate in a rotating system," in *Proceedings of the 8th BSME International Conference on Thermal Engineering*, Dhaka, Bangladesh, December 2018.

[29] M. Nawaz, S. Rana, I. H. Qureshi, and T. Hayat, "Three-dimensional heat transfer in the mixture of nanoparticles and micropolar MHD plasma with Hall and ion slip effects," *AIP Advances*, vol. 8, pp. 1–17, 2018.

[30] T. Hayat, M. B. Ashraf, H. H. Alsulami, and M. S. Alhuthali, "Three-dimensional mixed convection flow of viscoelastic fluid with thermal radiation and convective conditions," *PLoS One*, vol. 9, no. 3, Article ID e90038, 11 pages, 2014.

[31] G. Makanda, S. Shaw, and P. Sibanda, "Effects of radiation on MHD free convection of a Casson fluid from a horizontal circular cylinder with partial slip in non-Darcy porous

medium with viscous dissipation," *Boundary Value Problems*, vol. 2015, no. 75, pp. 1–14, 2015.

[32] I. Ullah, I. Khan, and S. Shafie, "MHD natural convection flow of Casson nanofluid over nonlinearly stretching sheet through porous medium with chemical reaction and thermal radiation," *Nanoscale Research Letters*, vol. 11, no. 527, pp. 1–15, 2016.

[33] Y. B. Kho, A. Hussanan, N. M. Sarif, Z. Ismail, and M. Z. Salleh, "Thermal radiation effects on MHD with flow heat and mass transfer in Casson nanofluid over A stretching sheet," *MATEC Web of Conferences*, vol. 150, pp. 1–6, 2018.

[34] D. Srinivasacharya and P. V. Kumar, "Effect of thermal radiation on mixed convection of a nanofluid from an inclined wavy surface embedded in a non-Darcy porous medium with wall heat flux," *Propulsion and Power Research*, vol. 7, no. 2, pp. 147–157, 2018.

[35] M. Hamid, M. Usman, Z. H. Khan, R. U. Haq, and W. Wang, "Numerical study of unsteady MHD flow of Williamson nanofluid in a permeable channel with heat source/sink and thermal radiation," *European Physical Journal Plus*, vol. 133, no. 527, pp. 1–12, 2018.

[36] T. Gangaiah, N. Saidulu, and A. V. Lakshmi, "The influence of thermal radiation on mixed convection MHD flow of a Casson nanofluid over an exponentially stretching sheet," *International Journal of Nanoscince and Nanotechnology*, vol. 15, no. 2, pp. 83–98, 2019.

[37] I. Waini, A. Ishak, and I. Pop, "Hybrid nanofluid flow and heat transfer over a nonlinear permeable stretching/shrinking surface," *International Journal of Numerical Methods for Heat & Fluid Flow*, vol. 29, no. 9, 2019.

[38] A. Haritha and V. Nagendramma, "MHD Casson fluid flow past a stretching cylinder subject to nanoparticles with Cattaneo-christove heat flux," *International Journal of Scientific Research*, vol. 8, no. 6, pp. 54–58, 2019.

[39] T. Hayat, S. Asghar, A. Tanveer, and A. Alsaedi, "Effects of Hall current and ion-slip on the peristaltic motion of couple stress fluid with thermal deposition," *Neural Computing and Applications*, vol. 31, no. 1, pp. 117–126, 2017.

[40] I. H. Qureshi, M. Nawaz, and A. Shahzad, "Numerical study of dispersion of nanoparticles in magnetohydrodynamic liquid with Hall and ion slip currents," *AIP Advances*, vol. 9, Article ID 025219, 2019.

[41] CH. B. Rania, N. Vedavathi, K. S. Balamurugan, and G. Dharmaiah, "Hall and ion slip effects on Ag-water based MHD nanofluid flow over a semi-infinite vertical plate embedded in a porous medium," *Frontiers in Heat and Mass Transfer (FHMT)*, vol. 14, no. 6, pp. 1–12, 2020.

[42] G. Mahanta and S. Shaw, "3D Casson fluid flow past a porous linearly stretching sheet with convective boundary condition," *Alexandria Engineering Journal*, vol. 54, no. 3, pp. 653–659, 2015.

[43] S. Shehzad, T. Hayat, and A. Alsaedi, "Three-dimensional MHD flow of Casson fluid in porous medium with heat generation," *Journal of Applied Fluid Mechanics*, vol. 9, no. 1, pp. 215–223, 2016.

[44] I.-C. Liu, H.-H. Wang, and Y.-F. Peng, "Flow and heat transfer for three-dimensional flow over an exponentially stretching surface," *Chemical Engineering Communications*, vol. 200, no. 2, pp. 253–268, 2013.

[45] M. V. S. Rao, K. Gangadhar, and P. L. N. Varma, "A spectral relaxation method for three-dimensional MHD flow of nanofluid flow over an exponentially stretching sheet due to convective heating: an application to solar energy," *Indian Journal of Physics*, vol. 92, no. 12, pp. 1577–1588, 2018.

[46] S. S. Motsa, P. J. Sibanda, M. Ngnotchouye, and G. T. Marewo, "A spectral relaxation approach for unsteady boundary-layer flow and heat transfer of a nanofluid over a permeable stretching/shrinking sheet," *Advances in Mathematical Physics*, vol. 2014, Article ID 564942, 10 pages, 2014.

[47] S. Shateyi, S. S. Motsa, and Z. Makukula, "On spectral relaxation method for entropy generation on a MHD flow and heat transfer of a Maxwell fluid," *Journal of Applied Fluid Mechanics*, vol. 8, no. 1, pp. 21–31, 2015.

[48] W. Ibrahim and T. Anbessa, "Mixed convection flow of nanofluid with Hall and ion slip effects using spectral relaxation method," *Journal of the Egyptian Mathematical Society*, vol. 27, no. 52, pp. 1–21, 2019.

[49] A. S. Idowu and B. O. Falodun, "Soret-Dufour effects on MHD heat and mass transfer of Walter's-B viscoelastic fluid over a semi-infinite vertical plate: spectral relaxation analysis," *Journal of Taibah University for Science*, vol. 13, no. 1, pp. 49–62, 2019.

[50] F. I. Alao, C. U. Boneze, and A. I. Fagbade, "Soret and dufour effects on heat and mass transfer of boundary layer flow over porous wedge with thermal radiation: bivariate spectral relaxation method," *American Journal of Chemical Engineering*, vol. 7, no. 1, pp. 7–21, 2019.

[51] T. Hayat, S. A. Shehzad, and A. Alsaedi, "MHD three-dimensional flow by an exponentially stretching surface with convective boundary condition," *Journal of Aerospace Engineering*, vol. 27, pp. 1–8, 2014.